

A Study on the Chain–Particle Interaction and Aspect Ratio of Nanoparticles on Structure Development of a Linear Polymer

Nilesh Patil,^{†,‡} Luigi Balzano,^{§,‡} Giuseppe Portale,^{||,§} and Sanjay Rastogi^{*,†,‡,§}

[†]Department of Materials, Loughborough University, Leicestershire LE11 3TU, U.K., [‡]Department of Chemical Engineering and Chemistry, Technische Universiteit Eindhoven, P.O. Box 513, 5600 MB Eindhoven, The Netherlands, [§]Dutch Polymer Institute, P.O. Box 902, 5600 AX Eindhoven, The Netherlands, ^{||}Department of Mechanical Engineering, Technische Universiteit Eindhoven, P.O. Box 513, 5600 MB Eindhoven, The Netherlands, and [¶]DUBBLE, CRG/ESRF, Netherlands Organization for Scientific Research (NWO), c/o ESRF BP 220, F-38043, Grenoble Cedex, France. [#]Present address: Dow Hyperlast, Dow Chemical Company Ltd., Birch Vale, High Peak, Derbyshire SK22 1BR, U.K.

Received March 23, 2010; Revised Manuscript Received July 8, 2010

ABSTRACT: The stability of metastable flow-induced precursor (FIPs) in the polymer melts in presence of nanoparticles, viz. single-walled carbon nanotube (SWCNT) and zirconia nanoparticles, is studied at, 142 °C, close to the equilibrium melting point of unconstrained extended chain crystals of linear polyethylene (PE). The results conclusively demonstrate the influence of chain–particle interactions, between PE and the nanoparticles, on the stretch of the long chains. With the applied flow, SWCNTs together with PE chains are observed to align along the flow direction, giving rise a strong streak like pattern along the equator. At the initial stages, intensity of the observed streak in the presence of SWCNTs is stronger than that for the neat polyethylene. The streak intensity stabilizes with time, where the time required for the stabilization depends on the amount of the dispersed nanotubes in the polymer matrix. On the contrary, in the presence of zirconia nanoparticles, where the chain–particle interactions between PE and the nanoparticles are weak the initially observed streak tends to disappear with time, where the time required is strongly dependent on the concentration of the nanoparticles in the polymer matrix. Thus, compared to the neat polymer, the presence of zirconia nanoparticles destabilizes the shish formation. The chain orientation along the flow direction is determined using Herman's orientation function and the length of the oriented chains (shish) by Ruland's streak analysis. On cooling, with the crystallization of the polymer, scattering develops along the meridian, indicating the development of folded chain crystals, where the oriented chains present along the flow direction provide the epitaxy matching thus suppressing the nucleation barrier. The meridional intensity (arising with the formation of crystals, called kebabs) at room temperature, shows strong dependence on the stable streak intensity (chain orientation along the flow direction, called shish) along the equator prior to cooling.

1. Introduction

The study of flow-induced precursors (FIPs) in initial stages of crystallization of polymers in the melts under the influence of flow field is important for achieving final properties in polymers. The applied flow field at a suitable temperature and deformation shear and strain rates promote the crystallization process and subsequently the resultant morphology associated with the final product. Many studies have shown the role of flow conditions in the formation of primary nuclei during the early stages of crystallization.^{1–14} Under flow, the polymer chains get aligned in the flow direction giving rise to maximum density fluctuation in the perpendicular direction as can be detected by time-resolved small-angle X-ray scattering (SAXS) techniques. Depending on the temperature and present heterogeneity the applied flow influences the molecular conformation in the polymer melt and may form stable primary nuclei. Time resolved SAXS techniques are applied in detecting the spatial arrangements and morphology developments due to rapid formation of primary nuclei in nanoseconds.¹⁵

The anisotropic precursor leads to the formation of shish-kebab morphology¹⁶ during the crystallization process under shear. The anisotropic structure influences the mechanical properties of

polymeric materials. The initial structures obtained after immediate shear can be metastable in nature and can undergo either crystallization or dissolution at high crystallization temperatures. The basis of formation of FIPs is a subject of interest in recent years.^{17–23,34,45–47} Above a critical strain rate under flow, the intense transition of polymer chains from random coil to extended chain conformation without appearance of the intermediate chain conformation is observed.²⁴

Keller et al.²⁵ speculated the existence of critical molecular weight M^* in the formation of oriented structures under shear flow. The study proved that the polymer chains longer than M^* can remain in extended state and oriented after deformation while short chains relax back to form random coil state due to short relaxation times. Furthermore, the crystallization of these extended chains leads to the shishes and epitaxial crystallization of coiled state leading to the formation of kebabs in later stages.

Hsiao et al.²⁶ studied the sheared polyethylene (PE) blend containing 2 wt % of ultrahigh molecular weight polyethylene (UHMWPE) and 98 wt % of low molecular weight PE. The scanning electron micrographs of a solvent extracted shear PE revealed the presence of shish-kebab structures with multiple shish. They stated that the disentanglements of UHMWPE in the blend, if any, were extremely low and further considered the hypothesis that the “entangled thread” upon stretching will show few straight sections with short thread lengths aligned parallel to

*Corresponding author. E-mail: S.Rastogi@lboro.ac.uk.

each other and remaining parts of thread reside in entanglements or globular sections. The multiple shish originate from stretched chain sections and kebabs originate from coiled chain section following the diffusion controlled crystallization process. Another study²⁷ suggests the presence of crystalline and amorphous regions within shish itself. Wu et al.²⁸ investigated the poly(vinylidene fluoride) (PVDF) fibers spun under stretch-hold deformation at room temperature. They obtained streak-like scattering in the equator and attributed those to the formation of microfibrils and microvoids, respectively.

In contrast to Cahn–Hilliard (CH) theory,²⁹ for spinodal decomposition which basically suggests the spontaneous growth of fluctuations indicative of thermodynamic instability,^{30,31} some studies,^{32–35} have provided possible explanation for the concept of spinodal decomposition as the extension of rigid segments having crystalline conformation caused by the conformational change of molecules from amorphous to crystalline state with the lowering of temperature. The simulation studies from Meakin et al.³⁶ provide the theoretical basis to the evolution of spinodal decomposition or the development of two-phase system. The presence of metastable liquid–liquid (LL) phase coexistence curve buried under the equilibrium liquid-crystal coexistence region forms a basis of spinodal dynamics in polymer melts. It is understood that polymer chain having restricted conformation will crystallize, but chain conformation alone cannot drive phase transition in melt condition; hence, it is usually coupled with density. The chain having the restricted conformation will pack more densely than the chain with random conformations. Thus, part of chain in dense region will be crystalline while amorphous in dilute region. The metastable (LL) phase is a result of conformation-density coupling and has been previously proved. This conformation–density coupling is vaguely believed to act as precursor to polymer crystallization. Hence, it is often considered that spinodal decomposition is not necessary to induce the shish-kebab structure formation.³⁷ The simulation study from Hu³⁸ and Dukovski and Muthukumar³⁹ proved the mechanism that governs the formation of shish-kebab structures. The study revealed the role of shishes as nucleating substrate in promoting the epitaxial crystallization of low molecular weight (M_w) chains to form kebabs. The simulation study clearly showed that the kebab growth was significantly influenced by the rate of addition or diffusion of chains. Kumaraswamy et al.⁴⁰ suggested the formation of oriented crystals on the basis of critical shear rate and shearing time. They showed stronger dependence of the shear rate than the shearing time on the orientation of crystals. Seki et al.⁴¹ proved the influence of high molecular weight chains exceeding the overlap concentration in the formation of oriented nuclei.

Ogino et al.⁴² stated that the critical concentration of high molecular weight (HMW) component in PE is two to three times larger than the overlap concentration of chain, C_{Rg}^* , indicating the role of entanglements of HMW PE chains in the formation of oriented structures. Matsuba et al.⁴³ further investigated the role of UHMW component on shish-kebab structure formation. The results suggested that the crystallization rate and the relaxation rate of ultrahigh molecular weight component have significant effect on the shish-kebab formation process.

Under flow conditions,^{44,45} Deborah numbers (De) associated with reptation and stretch can be defined as

$$De_{rep}, De_s > 1, \quad \lambda > \lambda^*(T) \quad (1)$$

where λ is a stretch ratio and λ^* is transition between two stretching regimes (i.e., the global configuration of the chain and the rotational isomerization (RI)) at temperatures well above the melting temperature, T_m , the chain segments are strongly oriented and the chain conformation becomes similar to that of

the crystalline state. Because of this, the critical fluctuations in the orientation and conformation of the chain segments are no longer required during flow. The application of the flow field therefore shifts the nucleation dynamics ultimately resulting in an increase of the observed nucleation rate. Van Meerveld et al.⁴⁵ applied four different approaches for determining the influence of reptation time (τ_{rep}) and stretch time (τ_s) to classify flow-induced crystallization. On the basis of their studies, it was concluded that strong chain stretching favored by the high molecular weight (HMW) governs the formation of shish-kebab structures.⁴⁶ The chain orientation and stretching associated with the HMW component was quantified using two Deborah numbers as⁴⁷

$$De_{rep}^{HMW} = \tau_{rep}^{HMW} \gamma^* \quad (2)$$

$$De_s^{HMW} = \tau_s^{HMW} \gamma^* \quad (3)$$

It is also resolved that the precursor formation occurs at temperatures close to the equilibrium melting point. One of the studies from Balzano et al.⁴⁷ proved the formation of FIPs at temperatures close to the equilibrium melting point. They investigated the problem with specially synthesized linear high density polyethylene (HDPE) having bimodal molecular weight distribution. The possibility to obtain the suspension of extended chain shish crystals close to equilibrium melting point of unconstrained extended chain crystals that requires the stretch of longest chains of MWD was demonstrated. Using the blends of UHMWPE and HDPE, Keum et al.⁴⁸ studied the formation and stability of shear induced shish-kebab structures in entangled melts at high temperature 142 °C. They confirmed the formation of shish without kebabs and absence of HDPE chains in shish formation. The thermal stability of oriented structure suggested the slow relaxation of stretched chains as governing factor for melting behavior of shishes. Recently, Kimata et al.⁴⁹ adopted the small-angle neutron scattering to show that long chains are not overrepresented in the shish relative to their concentration in the material as a whole. They concluded the presence of short and medium chains in the shish formation being greater than that of the long chains. Highly oriented and anisotropic structures can be formed by polymer molecules during shear in the presence of nucleating agents.^{50,51} Under flow, molecules of nucleating agent acts as point nuclei to form oriented crystals.^{52,53} The effects of nanoparticles (for instance, CNTs and silica) on polymer crystallization with and without flow have also been reported.^{54–60}

Lately,⁶¹ the SAXS/WAXD studies confirmed the nature and thermal stability of flow-induced crystallization precursor structures in blown LLDPE and HDPE/LLDPE films during constrained melting to prove the significance of high molar mass tail in the enhancement of highly oriented structures. Even though the last several decades count for excessive debates to understand the nucleation and growth behavior of polymers under shear flow with conventional theories and kinetics process associated with flow-induced crystallization, the basic mechanism responsible for nucleation and growth process in the very early stages of crystallization is still a matter of uncertainty. Using time-resolved SAXS technique, we aim to follow the governing factors in the formation of flow-induced oriented precursor formation by using polyethylene (PE) of broad molecular weight distribution (MWD). To elucidate the molecular nature of such oriented structures in the initial stages as a result of shish only, we chose the high temperature conditions ($T = 142$ °C) close to the equilibrium melting point of linear PE. At such high temperature condition, we attempt to resolve the issues related to chain alignment and high anisotropy as a result of chain extension. To understand stability of the precursors, two nanoparticles (SWCNT and zirconia) with different aspect ratio and molecular

interaction with polymer chain have been chosen. The chain orientation at high temperatures under strong shearing conditions is investigated.

2. Experimental Section

2.1. Materials and Sample Preparation. On the basis of our earlier work^{47,55} on polyethylene (PE), we have tried to exploit the topic for critical investigations to advance steps using the PE of broad molecular distribution (MWD). The PE (molecular weight $M_w = 246\,000$ g/mol, $M_n = 10\,100$ g/mol, $M_z = 1\,184\,000$ g/mol and polydispersity of $M_w/M_n = 24.2$ respectively) was kindly provided by the Dow Benelux B.V., The Netherlands. The sample obtained in powder form was polymerized using Zeigler-Natta catalyst in a slurry process. The nanoparticles used in the study consist of SWCNTs obtained from Unidym Inc., USA, having high aspect ratios (individual diameter of SWCNT ranging between ~0.8 and 1.2 nm with the individual length of SWCNT ranging between ~100 and 1000 nm) and aqueous suspension of nanosized yttria stabilized zirconia particles having average particle size of 20 nm were obtained from MEL Chemicals, UK. The suspension of SWCNTs was prepared and suspensions of both the nanoparticles were uniformly sprayed on PE powder as reported in other studies.⁶⁰

Samples in the form of flat disks of 400 μm thickness were prepared by compression molding the polyethylene powder. Samples thus prepared were investigated using time-resolved SAXS measurements. All the samples were mixed with Irganox 1010 to avoid the possible degradation while processing.

2.2. Small-Angle X-ray Scattering (SAXS) Instrumentation. A Linkam shear cell CSS 450 modified by replacing the quartz windows of shear cell with kapton windows to avoid X-ray absorption is adopted to apply steady shearing conditions. The shear cell is calibrated with the tolerance limit of $\pm 30 \mu\text{m}$ to have maximum contact of plates while shearing under preferred flow conditions. The flat disk-like samples are placed between the two plates of shear cell CSS 450 and are completely enclosed in the cell. In the melt, the sample having initial thickness of 400 μm is compressed to 200 μm to ensure the correct application of shear on the sample during measurements.

The two-dimensional (2D) time-resolved SAXS measurements are performed in DUBBLE/BM26B beamline at European Synchrotron Radiation Facility (ESRF), Grenoble, France. A 2D gas filled detector having resolution of 512 \times 512 pixels and 260 $\mu\text{m} \times 260 \mu\text{m}$ pixel size is employed to detect time-resolved small-angle X-ray scattering (SAXS) patterns for shear experiments. The sample to detector distance for SAXS is maintained at 6.057 m. The beamline consists of vacuum chamber in between the sample and detector to reduce the scattering and absorption from air. The wavelength of synchrotron radiation used in the reported SAXS experiments is 0.124 nm. The acquisition time of 10 s is used to acquire images with the dead time of 0.5 s between the adjacent images for required data transfer following the correction of intensity of the primary beam, sample thickness and absorption. The images are integrated to determine the scattered intensity (I) as a function of scattering vector (q). The integrated intensity as a function of time is defined as, $I_{\text{SAXS}}(t) = \int_{q_{\min}}^{q_{\max}} I(q,t) dq$, where q_{\max} and q_{\min} being the maximum and minimum of q values. The obtained intensity data is subtracted with intensity prior to the application of shear. The range of scattering vector in the SAXS measurements is kept between 0.05–0.5 nm⁻¹, where q is given by $q = 4\pi \sin \theta/\lambda$ (2θ being scattering angle).

2.3. Experimental Procedures. The chosen flow conditions are as follows: shear rate $\dot{\gamma} = 100/\text{s}$ for time duration $t_s = 1\text{ s}$. The temperature and shear plan is illustrated in Figure 1 for the studies, to summarize

- The sample is heated from room temperature to 160 °C at the heating rate of 30 °C/min

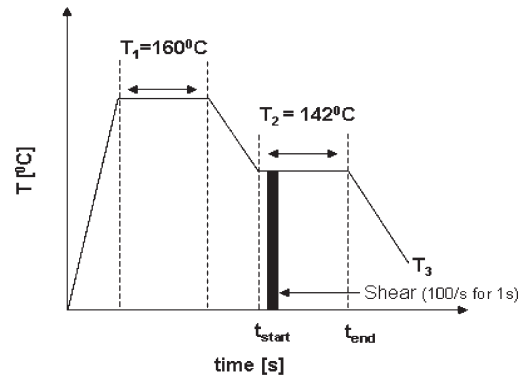


Figure 1. Schematic of the temperature and shear plan utilized in the present study. To study FIPs formation in the early stages of crystallization, the fast flow conditions with shear rate of 100/s for 1 s is applied at isothermal temperature of 142 °C. Here, T_1 represents temperature in the melt, i.e., $T_1 > T_m^* = 160$ °C for 5 min, where, $T_m^* = 141.2$ °C. T_2 represents isothermal temperature, i.e., $T_2 = 142$ °C and T_3 is 60 °C.

- The sample is held at 160 °C in the melt above equilibrium melting temperature for 5 min to remove complete melt history
- The sample is cooled to isothermal temperature (142 °C) at the cooling rate of 10 °C/min
- Shear rate $\dot{\gamma} = 100/\text{s}$ for time duration $t_s = 1\text{ s}$ is applied at 142 °C to follow development of FIP for 5 min at the isothermal condition
- The sample is cooled to $T = 60$ °C at the rate of 10 °C/min

The 2D SAXS patterns are recorded after every 10.5 s during complete temperature and shear plan.

2.4. Rheological Experiments. Advanced Rheometric Expansion System (ARES) with parallel plate geometry (25 mm of diameter) under nitrogen atmosphere is used in oscillatory shear mode. The experiments are performed at different temperatures in linear visco-elastic region. The storage modulus is followed as a function of angular frequency within the range of 0.01–100 rad/s. A low strain rate of 2.0% is applied in all the experiments. The obtained data is analyzed to determine the Deborah numbers associated with orientation and stretching of HMW chains.

3. Results and Discussions

3.1. Flow-Induced Precursors (FIPs) Formation (Shishes) in Broad Molecular Weight Distribution (MWD) Polyethylene at 142 °C under Strong Shear Conditions. Figure 2 depicts 2D SAXS patterns collected at selected times at the isothermal crystallization temperature (142 °C) close to the equilibrium melting point of linear polyethylene. The shear of $\dot{\gamma} = 100/\text{s}$ for $t_s = 1\text{ s}$ is applied and X-ray diffraction patterns are collected before and after the application of shear. The pattern collected just before shear at $t = 0\text{ s}$ at 142 °C shows the diffuse scattering in the vicinity of beamstop, suggesting the absence of any structure in melt. The first pattern collected after the application of shear, $t = 10\text{ s}$ shows scattering along the equator in the form of streak. The streak-like scattering is associated with the formation of metastable precursor that under suitable condition tends to grow to form stable shish. The pattern captured after $t = 50\text{ s}$ shows the appearance of strong streak-like scattering in the equator and the steady growth of intensity with time even at the high temperature. The increase in intensity with time suggests the growth of shish in the vicinity of equilibrium melting temperature. Considering these high temperatures, 142 °C, the stable growth of shish structure is associated with the formation of extended chain crystals, which tend to stabilize in the constrained condition.

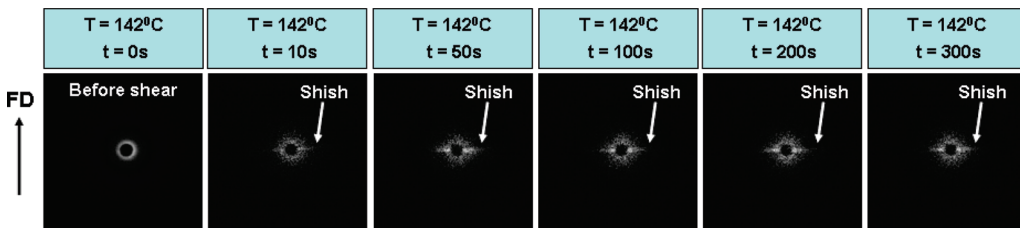


Figure 2. Selected 2D-SAXS patterns after the application of shear at isothermal temperature prior to crystallization above equilibrium melting point of linear PE. The intense needle-like scattering in the equator can be noticed at $t = 50$ s that gets sharp as a function of time.

Table 1. Relaxation Times and the Deborah Numbers of Reptation and Stretch of HMW Chains at 142 °C

shear rate (s^{-1})	shear time (s)	$a_T(T)$	E_a (kJ/mol)	τ_{rep}^{HMW} (s)	τ_s^{HMW} (s)	De_{rep}^{HMW}	De_s^{HMW}
100	1	2.439	29.659	56.651	0.0143	13 812	3.48

The streak-like scattering is the result of strong electron density variation occurring between the shish and polymer melt as polymer chains get aligned in flow direction with fast flow conditions. The streak-like scattering refers to the presence of shishes in the polymer melt at high temperature in the vicinity of the equilibrium melting point of linear polyethylene. Thermodynamic stability of the metastable structures can be understood by considering the anisotropy that causes the decrease in total free energy ($\Delta G_{total} < 0$). The energy associated with the formation of metastable flow-induced precursors can be related by eq 4.

$$\begin{aligned} \Delta G_{total}(L, D) \\ = - \left\{ \frac{\pi LD^2}{4} \right\} |\Delta g| + \left\{ \frac{\pi D^2}{2} \right\} \sigma_{end} + \pi LD\sigma_{lateral} \quad (4) \end{aligned}$$

Here, L and D are the length and diameter of FIPs. σ_{end} and $\sigma_{lateral}$ are the free energies at the end and lateral surfaces. Δg is the difference in the specific free energy of crystalline state and sheared polymer melt. The stability of precursor,⁶² is retained only if order of magnitude for L/D ratio exceeds the value of 10,

$$\left\{ \frac{\sigma_{end}}{\sigma_{lateral}} \right\} \sim 10 \quad (5)$$

From the rheological point of view, the flow reduces the chain conformations at high temperatures promoting the chain orientation in the direction of stretch. The governing criterion for chain orientation and stretch under suitable flow depends on the Deborah numbers. Considering the high molecular weight chains (HMW $\sim 1.184 \times 10^6$ g/mol) of polyethylene, it is expected that the chain orientation and stretch of high molar mass chains near equilibrium melting point (T_m^e), under strong shearing conditions ($\dot{\gamma} = 100/\text{s}$ for time duration $t_s = 1 \text{ s}$) for unconstrained extended chain crystals with no chain folding possibility is achieved. To determine the Deborah number of reptation (De_{rep}^{HMW}) and stretch (De_s^{HMW}) at 142 °C, the time–temperature superposition (TTS) principle is applied with the aid of rheology. To determine the relaxation times associated with chain reptation (τ_{rep}^{HMW}) and chain stretch (τ_s^{HMW}), the entanglement equilibration time, $\tau_e = 7 \times 10^{-9} \text{ s}$ at 190 °C and the entanglement molecular weight, $M_e = 828 \text{ g/mol}$ is assumed.⁶² Following the method described in literature and shown in the Supporting Information of this manuscript, for HMW chains ($M_z = 1.184 \times 10^6$ g/mol), the number of entanglements per unit chain (Z), relaxation times for reptation and stretch are determined. The Arrhenius type of temperature dependence with activation energy E_a =

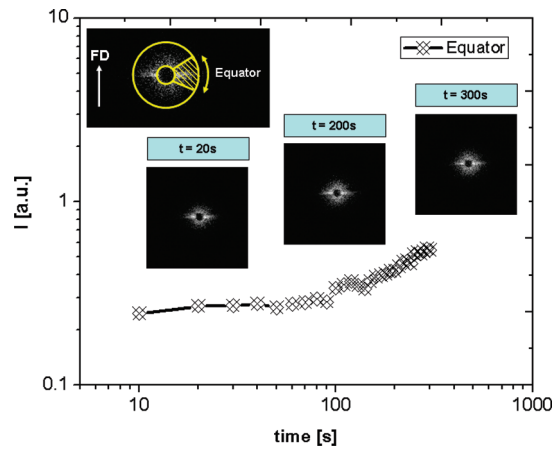


Figure 3. Integrated intensity obtained as a result of needle-like scattering in the equator from the SAXS analysis. The intensity has been integrated along the cake as shown in the shaded region. The plot consists of patterns acquired after selected time in the isothermal temperature condition. The result shows the presence of clear needle-like structures in the polymer melt. The intensity increases as the function of time suggesting the growth of FIPs.

29.659 kJ/mol is found for the horizontal shift factor (a_T) at $T = 142$ °C. The vertical shift factor (b_T) does not show strong temperature dependence. The shift factors for different temperatures are determined experimentally on the application of TTS principle to storage modulus (G') curves obtained in the frequency spectrum of 0.01 to 100 rad/s. The Arrhenius activation energy for TTS principle can be expressed⁶³ as

$$a_T(T) = \exp \left[\frac{E_a}{R} \left(\frac{1}{T} - \frac{1}{T_o} \right) \right] \quad (6)$$

where E_a is Arrhenius activation energy, $a_T(T)$ is shift factor at absolute temperature, R is gas constant (8.314 J/mol·K⁻¹), $T = 415$ K is absolute temperature and $T_o = 463$ K is reference temperature. The obtained shift factor at 142 °C is considered while using eqs 2 and 3 to calculate the De for HMW chains at 142 °C. The calculated relaxation times and Deborah numbers for the applied shear rate are reported in Table 1.

Figure 3 shows intensity build up at the equator after application of strong shear ($\dot{\gamma} = 100/\text{s}$, $t_s = 1 \text{ s}$). The steady growth of SAXS intensity and the stabilization of flow-induced crystals in the vicinity of equilibrium melting point of the polymer are observed as a function of time. The intensity tends to grow with time after the application of

shear suggesting the growth of shishes. The evolution of azimuthal peak at the equator after the application of shear is shown in Figure 4. Immediately after the application of shear the azimuthal peak tends to broaden and becomes sharp. The scattering obtained in the equator as a function of azimuthal

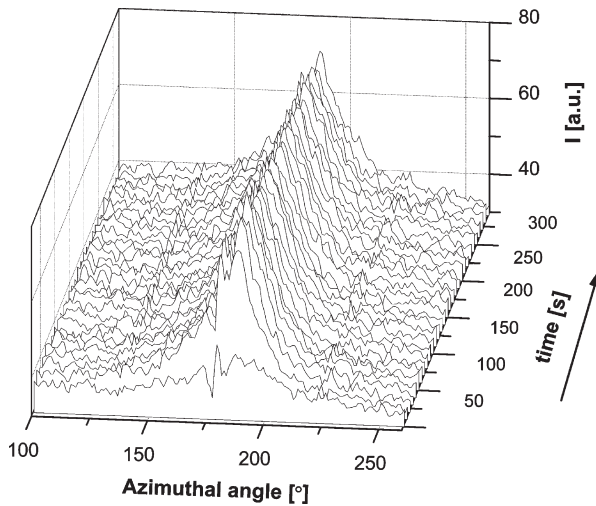


Figure 4. Time resolved evolution of azimuthally integrated intensity at the equator in the neat polymer. The peak in the equator ($\theta = 180^\circ$) is the result of scattering in the equator associated with the metastable flow-induced precursors (FIPs) obtained at isothermal temperature ($T = 142^\circ\text{C}$) after the application of strong short-term shear ($\dot{\gamma} = 100/\text{s}$, $t_s = 1\text{ s}$).

angle is used in determination of shish length as demonstrated later in the paper.

3.2. Stability of FIPs at 142 °C in Broad Molecular Weight Distribution (MWD) Polyethylene in the Presence of Nanoparticles. The stability of flow-induced precursors is studied in the presence of two different nanoparticles, having different chain–particle interaction for polyethylene chains. For example, due to similarity at the atomistic level of carbon nanotubes and polyethylene chains, a strong interaction between SWCNT and PE is anticipated. Moreover, the higher aspect ratio of SWCNTs will also favor the molecular interaction between SWCNTs and polyethylene chains. The strong interaction would provide easy stretchability of polyethylene chains with the SWCNTs. On the contrary, due to poor chain–particle interaction between zirconia and polyethylene, the polyethylene chains adhered to the zirconia nanoparticles will tend to slip under shear. Further, the entropy driven relaxation process will tend to transform the stretched chains into random coil. To investigate such a possibility the following experiments are performed.

The samples of physically dispersed nanoparticles on the polymer powder are subjected to strong shearing conditions, defined in Figure 1. 2D-SAXS patterns for selected times before and after the application of shear is acquired. Figure 5a shows the composite of 2D-SAXS patterns recorded at different times after shear in the presence of different wt % of SWCNTs in the polymer matrix. Compared to the neat polyethylene (Figures 2 and 3) the scattered intensity just after the shear is found to be much higher. This suggests that the presence of SWCNTs enhances the formation of flow-induced

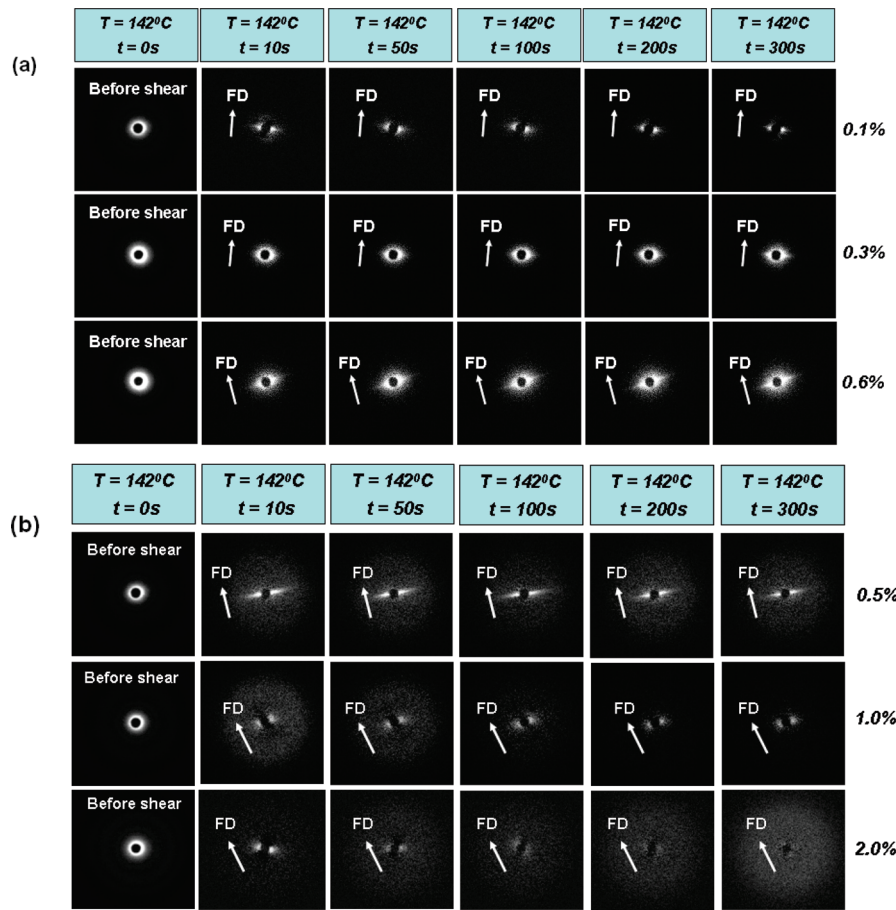


Figure 5. 2D-SAXS patterns acquired at selected times at isothermal temperature condition ($T = 142^\circ\text{C}$). The images are acquired at 142 °C before and after application of shear ($\dot{\gamma} = 100/\text{s}$, $t_s = 1\text{ s}$): (a) composite of SAXS patterns of polymer melt in the presence of increasing SWCNT concentration; (b) patterns of polymer melt in presence of different concentration of zirconia nanoparticles.

Table 2. Estimated Surface Area of Different Concentration of Nanoparticles Dispersed in 1 g of Polyethylene (PE)

SWCNT concn (wt %)	surface area (m ² /g)	zirconia concn (wt %)	surface area (m ² /g)
0.1	40.04	0.5	0.99
0.3	119.40	1.0	1.99
0.6	240.24	2.0	3.97

precursor immediately after the application of shear. However, with time the intensity along the equator tends to decrease suggesting dissolution of the precursors with time. Such a phenomenon is apparent in the polyethylene matrix having 0.1 wt % of SWCNTs. With increase in the concentration of SWCNTs, from 0.1 to 0.3 wt %, transformation of streak-like scattered intensity in to broad maxima along the equator is observed. The broadening suggests increase in the number of shishes in the polymer melt. With time, after the applied shear, the intensity of the broad equatorial maxima decreases before the scattered intensity stabilizes and remains constant over the period of isothermal condition. The decrease in scattered intensity after the applied shear suggests dissolution of some metastable flow-induced precursors. While on increasing the concentration of SWCNTs from 0.3 to 0.6 wt %, the broad intensity along the equator after shear tends to increase. It is to be realized that in a homogeneously dispersed SWCNTs in polymer matrix, 0.6 wt % of SWCNTs correspond to percolation threshold that results in the formation of stable overlapping network of SWCNTs. The presence of such a network will provide the maximum surface of favorable heterogeneous nuclei for the crystallization of polyethylene. Considering the anisotropic distribution of intensity, mainly perpendicular to the flow direction, the SWCNTs are likely to align along the flow direction. Thus, promoting the alignment of anchored chains on SWCNTs. An efficient chain stretch requires sharing of a chain between two or more SWCNT. Such a probability would be highest for the long molecules in the broad molar mass distribution polymer. Further the high relaxation times of the high molar mass component under stress will also favor the chain orientation and the formation of extended chain crystals.

Figure 5b shows the 2D-SAXS patterns of polymer melt in the presence of zirconia nanoparticles. The nanoparticle size of zirconia (20 nm) provide very high surface to volume ratio, thus a good probability for a chain to anchor with different nanoparticles. At the low concentration of zirconia (0.5 wt %) after application of shear strong equatorial scattering is observed. However, the scattering tends to decrease with time suggesting dissolution of shish. It is interesting to note that with increasing concentration of zirconia nanoparticles, though the surface area of heterogeneous nuclei increases dramatically (as shown in Table 2), the arising equatorial intensity due to shish formation decreases considerably. Unlike PE having 0.6 wt % of SWCNTs, where the streak intensity increases with time, in the higher concentration of zirconia the intensity along the equator vanishes with time suggesting complete loss of the detectable oriented structure arising due to the applied flow.

Figure 6 shows integrated SAXS profiles obtained by integrating intensity along the equator at different concentrations of nanoparticles after $t = 300$ s of the applied shear at isothermal condition, 142 °C. The changes in the intensity along q ($q = 4\pi(\sin \theta)/\lambda$) are observed with the increasing concentration of nanoparticles. On increasing concentration of SWCNTs, the overall scattered intensity increases. The scattered intensity for 0.5 wt % of zirconia concentration in PE is more compared to the neat PE. However, the intensity

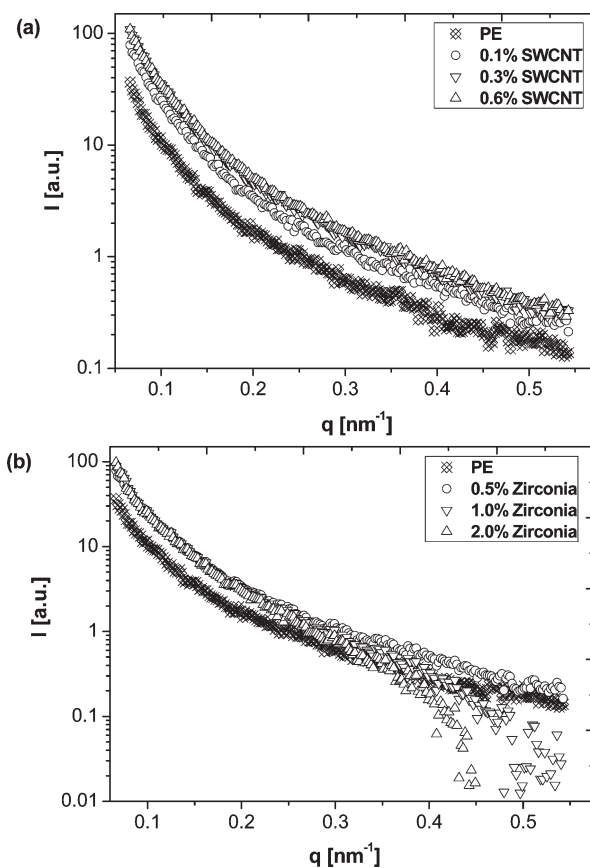


Figure 6. Scattered intensity in the equator obtained after application of shear ($\dot{\gamma} = 100$ s⁻¹, $t_s = 1$ s) for the 2D-SAXS patterns of polymer melt in the presence of different concentration of nanoparticles collected after $t = 300$ s of isothermal crystallization at 142 °C (a) in presence of SWCNTs and (b) in presence of zirconia nanoparticles. The intensity at the y-axis is the integrated intensity in logarithmic scale, where, $q = 4\pi(\sin \theta)/\lambda$, 2θ is the scattering angle.

at higher q -values is significantly decreased in polyethylene containing higher concentration of zirconia nanoparticles suggesting decrease in streak length.

For quantitative comparison between the arising intensity due to shear deformation in the presence of nanoparticles, the scattering data after shear is subtracted from the scattering data prior to deformation.

Figure 7 shows changes in the integrated 2D-SAXS intensity of equatorial region as a function of time at an isothermal condition, 142 °C, after the application of shear. It is evident that in all samples with the application of shear, intensity along the equator increases, favoring the formation of flow-induced precursors. After cessation of the shear while in the neat polyethylene the intensity continues to increase gradually with time, in the presence of the nanoparticles the intensity (though higher initially) tends to decrease with the exception for polymer composite having 0.6 wt % of SWCNTs. Compared to the SWCNT, strong decrease in the scattered intensity is observed in the presence of zirconia, highlighting the influence of interfacial free energy in the stabilization of oriented extended chain crystals at these high temperatures. A cause for the stabilization of the oriented structures close to the equilibrium melting point can be associated with the presence of local constraints on the extended chain crystals, even after cessation of the shear. Growth of shish in the neat polyethylene may also arise due to change in the pressure at the vicinity of the growth front of shish on crystallization. The shish growth is likely to be

favored because of the presence of the high molar mass in the broad molar mass distribution of polyethylene. However,

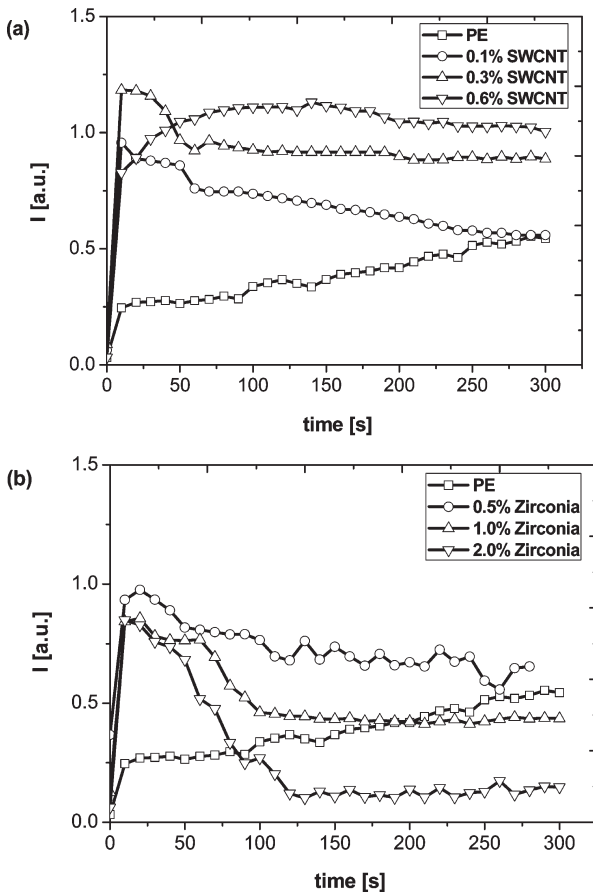


Figure 7. Equatorial integrated intensity obtained from SAXS data analysis as a function of time: (a) in the presence of SWCNTs; (b) in the presence of zirconia nanoparticles. The rapid rise in the intensity immediately after the application of shear is noticed in the presence of nanoparticles in polymer melts at isothermal temperature ($T = 142^\circ\text{C}$). The intensities are subtracted with the intensity prior to the application of shear. The subtraction is performed to follow the development of resultant intensity due to structure formation after the application of flow.

with the performed studies the possibility of the involvement of low molar mass component in the shish, during the shish growth process after cessation of the flow, cannot be elucidated nor ignored. Schematic presentation arising from the obtained information on the shish formation in the neat PE and PE with the nanofillers is depicted in Figure 8. Considering the requisite of chain overlap on the fillers to transfer the stresses on shear, shish formation at the initial stages should comprise of high molar mass chains.

Compared to the neat PE and PE with SWCNTs, the polymer melt in the presence of zirconia nanoparticles at the isothermal condition 142°C , shows different scenario, see Figure 7. The high electron density contrast in the equator observed at the early stages of crystallization at low zirconia concentration decreases with increase in zirconia concentration in polymer. The increasing concentration of zirconia nanoparticles is found to perturb chain extension in polymer melt. The rise of intensity in the early stages is followed by the decrease of intensity indicating the dissolution of precursors (shishes) in polymer melt. It is generally assumed that local anisotropic crystalline structures are formed due to high molecular orientation especially near particles. In the case of zirconia nanoparticles, it may be anticipated that poor chain–particle interaction between zirconia nanoparticles and polymer chain affects the chain orientation and with time, the chain dislocate through the surface of zirconia nanoparticles further prohibiting the stable shish formation.

3.3. Orientation Function of Shish in the Neat Polymer and in the Presence of Nanoparticles. The information about orientation in preferred direction is extracted using the Herman's orientation function in the polymer melt sheared near the equilibrium melting point of unconstrained extended chain crystals requiring the stretch of longest chains of MWD. The extensive analysis of intensity as a function of azimuthal angle from SAXS data is performed to obtain orientation parameter. For a given 2D-SAXS pattern, the orientation parameter is determined using Herman's orientation function^{64,65} as

$$f_h = \left\{ \frac{(3\langle \cos^2 \phi \rangle - 1)}{2} \right\} \quad (7)$$

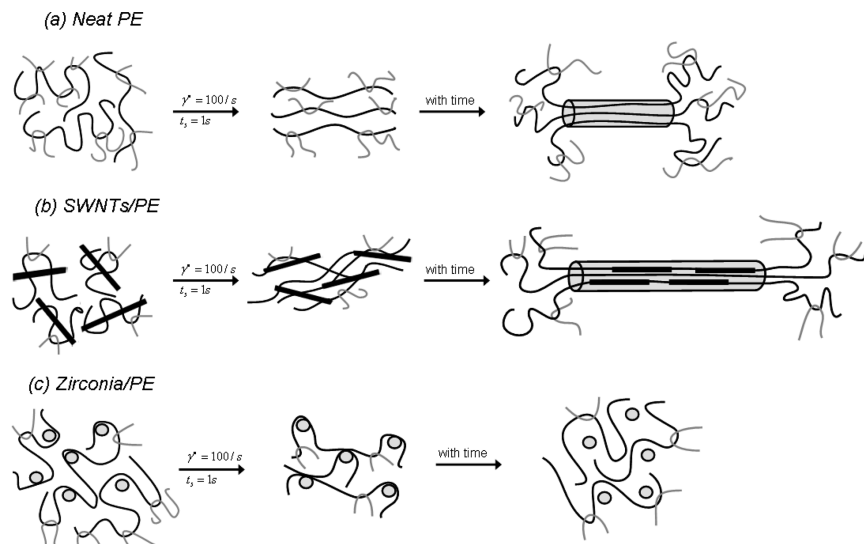


Figure 8. Shish formation in the neat polyethylene and PE in the presence of nanofillers: (a) the growth of shish formation in neat polyethylene depicting the stretch of long chain in broad molar mass distribution; (b) in the presence of SWCNTs, the shish formation is promoted due to anchoring of polymer chains on SWCNTs; (c) in the presence of zirconia, the shish formation is perturbed due to weak chain–particle interactions.

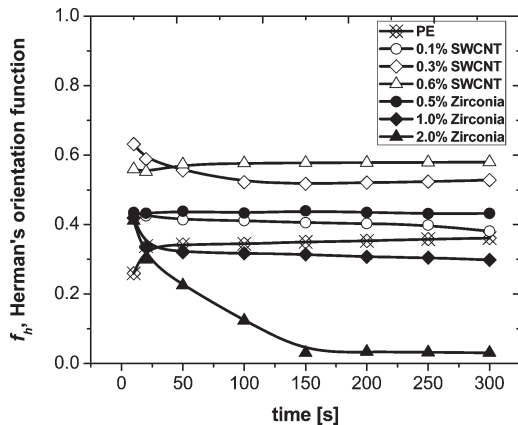


Figure 9. Calculated Herman's orientation function for the different concentration of nanoparticles in polymer melt at isothermal temperature ($T = 142^\circ\text{C}$) prior to crystallization.

The mean-square cosine of azimuthal angle can be described by eq 8,

$$\cos^2 \phi = \frac{\int_0^{\pi/2} I(\theta) \cos^2 \theta \sin \theta d\theta}{\int_0^{\pi/2} I(\theta) \sin \theta d\theta} \quad (8)$$

The cake corresponding to one quadrant ($\theta = 90^\circ$ to 180°) of azimuthally integrated 2D-SAXS patterns in anticlockwise direction is considered for the estimation of orientation functions in all the samples. The data analysis in the performed conditions gives the values of Herman's orientation function (f_h), i.e., $f_h = 1$, when scattered intensity is concentrated in the equator (i.e., perpendicular to flow direction in 2D-SAXS patterns, in otherwords, considered to be the signature of chain orientation in our case), $f_h = -0.5$, when scattered intensity is concentrated in the meridian (i.e., parallel to flow direction in 2D-SAXS patterns), and $f_h = 0$, when scattered intensity is diffused (isotropic in nature) and spread across the pattern.

Figure 9 shows the Herman's orientation function estimated using the obtained 2D-SAXS data analysis. The data shows good agreement with the obtained 2D-SAXS images (refer to Figure 5, parts a and b). The increased concentration of SWCNTs favors the chain orientation process in the polymer melt. On the other hand, the increased concentration of zirconia nanoparticles perturbs the chain orientation in the polymer melt. The decrease of chain orientation in the presence of zirconia nanoparticles is due to dissolution of metastable precursors. The entropy driven process of chain relaxation in the stretched chains is strongly influenced in the presence of SWCNTs. This results in the higher orientation function along the chain axis. The decrease in chain orientation in the presence of zirconia nanoparticles is caused by the poor chain–particle interaction between zirconia and polyethylene chains that promotes entropy driven chain relaxation of the stretched chains.

3.4. Estimation of Shish Length in the Neat Polymer and in the Presence of Nanoparticles. The time evolution of flow-induced precursors (shish) formation was further investigated to determine changes in the length of shish (L) using Ruland's streak analysis.^{66–68} The method was originally used to determine the size and orientation distribution of longitudinal voids in polymer and carbon fibers in real space. The method can be used to estimate the shish length based on the equatorial scattering in the reciprocal space.

The integral width of angular distribution of the scattered intensity B_{obs} was used to estimate the true width of the

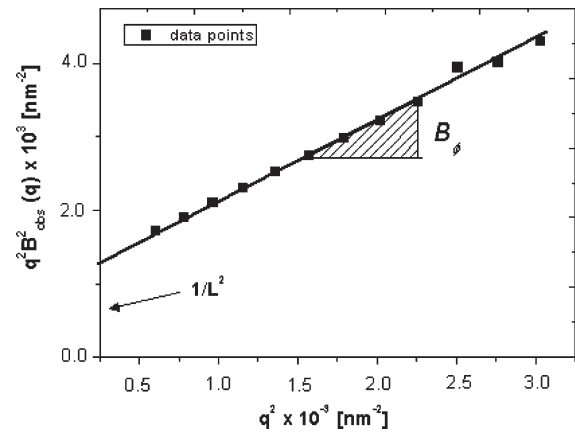


Figure 10. Plot of $q^2 B_{obs}^2$ vs q^2 used for the calculation of shish length (L) and misorientation (B_ϕ). The orientation distribution is approximated using Lorentzian fit of observed azimuthal integral breadth as a function of scattering vector (q).

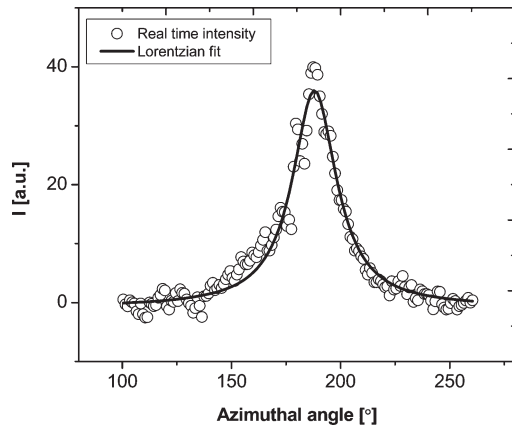


Figure 11. Example of typical Lorentz corrected distribution of scattered intensity in the equator as a function of azimuthal angle for specific value of scattering vector (q).

orientation distribution B_ϕ (misorientation) and the average length (L) of the shishes aligned in the direction of c -axis. The parameters obtained from Ruland's streak method were used to analyze the scattered equatorial streak. The azimuthally distributed scans of intensities at different q values were analyzed using Lorentz function to yield the average width of angular distribution. The width of the equatorial streaks in the reciprocal space can be related to obtain the length of shish (L). The relationship between the L and B_ϕ can be approximated as,

$$q^2 B_{obs}^2 = \frac{1}{L^2} + q^2 B_\phi^2 \quad (9)$$

The relationship gives linear plot obtained between $q^2 B_{obs}^2$ and q^2 as shown in Figure 10.

The shish length (L) and degree of misorientation (B_ϕ) are determined through the linear least-squares fitting applied to our data. In the relation, $q = 4\pi(\sin \theta)/\lambda$, θ being the scattering angle whereas q is the scattering vector and λ is wavelength. The length of shish (L) is determined from the intercept of the linear plot. The interpretation of “ L ” for shish is considered to be orderly aligned in the direction of c -axis.

The typical intensity distribution obtained in the equator as a function of azimuthal angle is shown in the Figure 11. To get precise integral width of the angular distribution, the

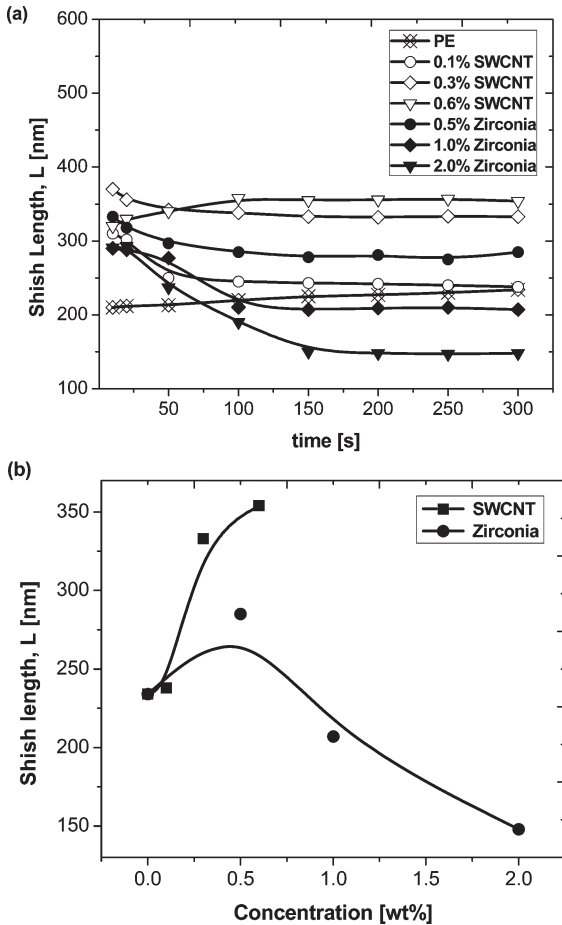


Figure 12. Estimated shish length of polymer melts in the presence of nanoparticles. Key: (a) deviation in shish lengths as a function of time at isothermal temperature, $T = 142\text{ }^{\circ}\text{C}$; (b) variation in shish length with increasing concentration of nanoparticles in polymer at $T = 142\text{ }^{\circ}\text{C}$ after $t = 300\text{ s}$ of the application of shear ($\dot{\gamma} = 100/\text{s}$, $t_s = 1\text{ s}$).

azimuthal peak in the equator is fitted with Lorentz correction method. The shish lengths as a function time at isothermal crystallization temperature ($T = 142\text{ }^{\circ}\text{C}$) are obtained in PE in the presence of nanoparticles.

Figure 12a shows variation in shish length at $142\text{ }^{\circ}\text{C}$ after the application of shear ($\dot{\gamma} = 100/\text{s}$, $t_s = 1\text{ s}$). The steady rise of shish length (up to 20 nm) in the neat polymer, at isothermal condition is observed. In the presence of nanoparticles, the shish length is found to vary from $t = 0\text{ s}$ to 150 s and becomes stable after 150 s . With increasing concentration of SWCNTs in polymer melt, for an example in the presence of 0.6 wt % SWCNTs at the end of isothermal condition, $142\text{ }^{\circ}\text{C}$, the shish length is found to increase up to $\sim 120\text{ nm}$. The rapid decrease in the shish length due to chain relaxation is observed immediately after the application of shear. In the presence of zirconia nanoparticles, compared to neat polymer, the shish length decreases indicating the dissolution of metastable precursors in polymer melt.

Figure 12b shows a comparison of average shish length at different concentration of nanoparticles at isothermal temperature, $T = 142\text{ }^{\circ}\text{C}$. The small amount of SWCNTs leads to the higher chain extension, eventually increasing the shish length by several tens of nanometers. The spherical rigid zirconia nanoparticles are found to decrease the average shish length with the increase in concentration. The 2.0 wt % zirconia in polymer melt showed large extent of disorientation at the end of isothermal temperature.

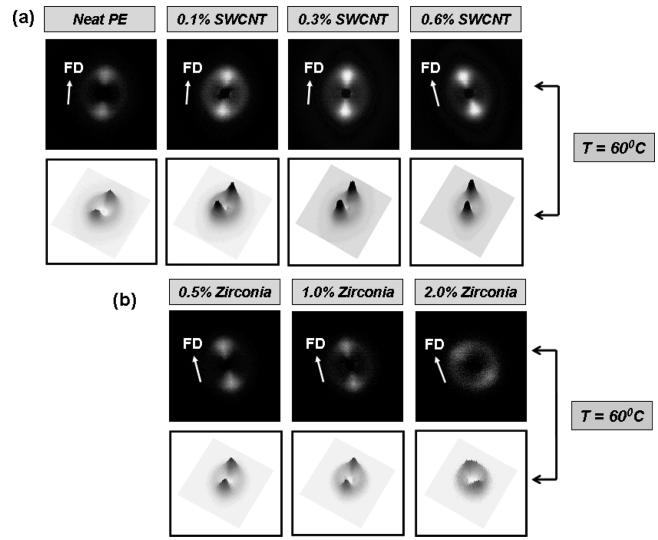


Figure 13. 2D-SAXS patterns obtained after cooling at $T = 60\text{ }^{\circ}\text{C}$ for the polymer and in presence of different concentration of nanoparticles: (a) increase in the oriented structure formation with the increase of SWCNT concentration; (b) decrease in the oriented structure formation with the increase in zirconia particles in polymer.

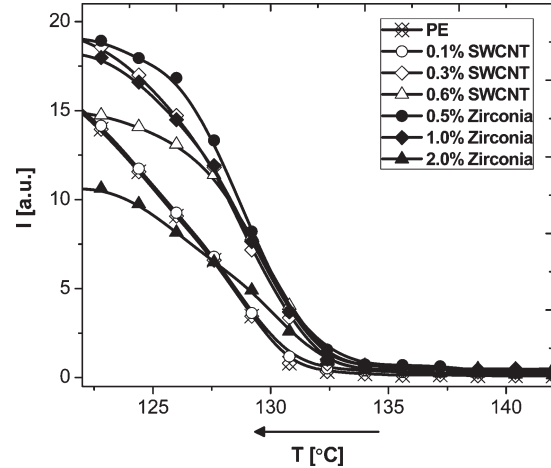


Figure 14. Integrated intensity against temperature for different samples on cooling. The intensity data is subtracted with intensity prior to application of shear. The earlier onset in intensity can be noticed in the presence of nanoparticles.

3.5. Crystallization on Cooling. Figure 13 shows patterns collected at $60\text{ }^{\circ}\text{C}$ after cooling the sample from 142 to $60\text{ }^{\circ}\text{C}$. The crystallized oriented chains (shish) provide perfect epitaxy matching for crystal growth (kebabs). The patterns in Figure 13a show steady growth of kebab formation with the increase in SWCNT concentration. The higher amount of oriented lamellae in later stages is the outcome of stable shishes present in the polymer melt after the application of shear. The increase in kebab formation with the increase of SWCNT concentration confirms precursor formation. Contrary to SWCNTs, the anisotropic kebab formation is found to decrease with increase in concentration of zirconia nanoparticles (refer Figure 13b). The results indicate decrease in the flow-induced precursor formation and/or chain orientation in polymer in the presence of zirconia nanoparticles at higher concentrations. The decrease in the precursor formation influences the radial growth of lamellae (kebabs) perpendicular to central core (shish).

Figure 14 shows the change in the integrated intensity as a function of temperature while cooling from 142 to $60\text{ }^{\circ}\text{C}$. As

expected, the nanoparticles, in general, are found to accelerate crystallization kinetics, apparent from the slope of integrated intensity. On cooling, the intensity rises at higher temperature; this refers to early onset of crystallization in the presence of nanoparticles. The accelerated crystallization kinetics depends on shear rate, temperature, melt memory and influence of additives etc. In our case, we expect the accelerated crystallization kinetics is a result of combined effects of shear rate ($\dot{\gamma} = 100/\text{s}$ for time duration $t_s = 1 \text{ s}$), high shearing temperature ($T = 142^\circ\text{C}$), broad molar mass of the polymer, and influence of nanoparticles (SWCNT and zirconia).

4. Conclusions

The present study investigates the formation of flow-induced precursors (FIPs) in a polymer melt having broad molar mass distribution near the equilibrium melting point of unconstrained extended crystals of linear PE. The time-resolved X-ray scattering (SAXS) technique is applied to follow stability of precursors at the isothermal temperature prior to crystallization. The precursor formation in the presence of SWCNTs and zirconia nanoparticles is compared with the neat PE. The presence of SWCNTs promotes the precursor formation due to increase in the chain relaxation time favoring the stability of oriented metastable structure. In contrast, the presence of zirconia nanoparticles perturbs the precursor formation compared to the neat polymer. The calculated orientation function reveals the influence of nanoparticles on chain orientation. The presence of SWCNTs promotes the chain alignment in flow direction leading to the development of flow-induced precursors that eventually orients the crystals toward the chain axis. The zirconia nanoparticles at higher concentration showed the random orientation of crystals, indicating the perturbation of precursor formation. The Ruland's streak method is further utilized to estimate the length of shishes. The presence of small amount of SWCNTs ($\sim 0.6 \text{ wt \%}$) enhances the average shish length to $\sim 120 \text{ nm}$ in polymer melt. With the increase in concentration, the spherical zirconia nanoparticles are found to decrease the average shish length up to $\sim 90 \text{ nm}$.

Acknowledgment. The authors like to thank ESRF and Netherlands Organization of Scientific Research (NWO) for providing beamtimes for the present study. The authors also thank Mr. Frederik Gemoets from Plastic Research Division, Dow Benelux B.V., for providing GPC data for supplying the PE used in the study.

Supporting Information Available: Text giving further information on calculation of the Deborah number described in the main text and a table of rheological parameters for PE at different temperatures. This material is available free of charge via the Internet at <http://pubs.acs.org>.

References and Notes

- (1) Mackley, M. R.; Frank, F. C.; Keller, A. *J. Mater. Sci.* **1975**, *10*, 1501–1509.
- (2) Binsbergen, F. L. *Nature* **1966**, *211*, 516–517.
- (3) Calvert, P. *Nature* **1975**, *255*, 195–196.
- (4) Janeschitz-Kriegl, H.; Ratajski, E.; Stadlbauer, M. *Rheol. Acta* **2003**, *42*, 355–364.
- (5) Graham, R. S.; Olmsted, P. D. *Phys. Rev. Lett.* **2009**, *103*, 115702–4.
- (6) Ward, I. M. *Structure and Properties of Oriented Polymers*; Chapman and Hall: London, 1997.
- (7) Bassett, D. C. *Principles of Polymer Morphology*; Cambridge University Press: Cambridge, U.K., 1981.
- (8) (a) Flory, P. J. *J. Chem. Phys.* **1947**, *15*, 397–408. (b) Flory, P. J. *Statistical Mechanics of Chain Molecules*; Interscience: New York, 1969.
- (9) Bashir, Z.; Odell, J. A.; Keller, A. *J. Mater. Sci.* **1986**, *21*, 3993–4002.
- (10) Cappuccio, G.; Ward, I. M. *Nature Phys. Sci.* **1973**, *243*, 143–143.
- (11) Ziabicki, A. *Fundamentals of Fiber Formation*; Wiley-VCH: New York, 1976.
- (12) Janeschitz-kriegl, H.; Ratajski, E. *Polymer* **2005**, *46*, 3856–3870.
- (13) Koscher, E.; Fulchiron, R. *Polymer* **2002**, *43*, 6931–6942.
- (14) Strobl, G. *The Physics of Polymers*; Springer-Verlag: Berlin, 1997.
- (15) Gee, R. H.; Fried, L. E. *J. Chem. Phys.* **2003**, *118*, 3827–3834.
- (16) Pennings, A. J.; Kiel, A. M. *Kolloid-Z. Z. Polym.* **1965**, *205*, 160–162.
- (17) (a) Somani, R. H.; Yang, L.; Hsiao, B. S. *Physica A* **2002**, *304*, 145–147. (b) Somani, R. H.; Yang, L.; Hsiao, B. S.; Agarwal, P. K.; Fruitwala, H. A.; Tsou, A. H. *Macromolecules* **2002**, *35*, 9096–9104.
- (18) Azzurri, F.; Alfonso, G. C. *Macromolecules* **2005**, *38*, 1723–1728.
- (19) Janeschitz-Kriegl, H.; Eder, G. *J. Macromol. Sci., Part B* **2007**, *46*, 591–601.
- (20) Garcia-Gutierrez, M. C.; Alfonso, G. C.; Riekel, C.; Azzurri, F. *Macromolecules* **2004**, *37*, 478–485.
- (21) Fernandez-Ballester, L.; Gough, T.; Meneau, F.; Bras, W.; Ania, F.; Balta-Calleja, F. J.; Kornfield, J. A. *J. Synchrotron Radiat.* **2008**, *15*, 185–190.
- (22) (a) Kanaya, T.; Takayama, Y.; Ogino, Y.; Matsuba, G.; Nishida, K. *Lect. Notes Phys.* **2007**, *714*, 87. (b) Hayashi, Y.; Matsuba, G.; Zhao, Y.; Nishida, K.; Kanaya, T. *Polymer* **2009**, *50*, 2095–2103.
- (23) (a) Schultz, J. M.; Hsiao, B. S.; Samon, J. M. *Polymer* **2000**, *41*, 8887–8895. (b) Samon, J. M.; Schultz, J. M.; Hsiao, B. S. *Polymer* **2002**, *43*, 1873–1875.
- (24) (a) De Gennes, P. G. *J. Phys. Chem.* **1974**, *60*, 5030–5042. (b) De Gennes, P. G. *Scaling Concepts in Polymer Physics*; Cornell University Press: Ithaca, NY, 1979.
- (25) Keller, A.; Kolnaar, H. W. *Mater. Sci. Technol.* **1997**, *18*, 189–268.
- (26) Hsiao, B. S.; Yang, L.; Somani, R. H.; Avila-Orta, C. A.; Zhu, L. *Phys. Rev. Lett.* **2005**, *94*, 117802–4.
- (27) (a) Zhang, C.; Hu, H.; Wang, D.; Shouke, Y.; Han, C. C. *Polymer* **2005**, *46*, 8157–8161. (b) Zhang, C.; Hu, H.; Wang, X.; Yao, Y.; Dong, X.; Wang, D.; Wang, Z.; Han, C. C. *Polymer* **2007**, *48*, 1105–1115.
- (28) Wu, J.; Schultz, J. M.; Yeh, F.; Hsiao, B. S.; Chu, B. *Macromolecules* **2000**, *33*, 1765–1777.
- (29) Cahn, J. W.; Hilliard, J. E. *J. Chem. Phys.* **1958**, *28*, 258–267.
- (30) Gee, R. H.; Lacevic, N.; Fried, L. E. *Nature Mat.* **2006**, *5*, 39–43.
- (31) Matsuba, G.; Kanaya, T.; Saito, M.; Kaji, K.; Nishida, K. *Phys. Rev. E* **2000**, *62*, R1497–R1500.
- (32) (a) Schultz, J. M.; Lin, J. S.; Hendricks, R. W.; Petermann, J.; Gohil, R. M. *J. Polym. Sci.: Polym. Phys.* **1981**, *19*, 609–620. (b) Petermann, J.; Gohil, R. M.; Schultz, J. M.; Hendricks, R. W.; Lin, J. S. *J. Polym. Sci.: Polym. Phys.* **1982**, *20*, 523–534.
- (33) Olmsted, P. D.; Poon, W. C. K.; McLeish, T. C. B.; Terrill, N. J.; Ryan, A. J. *Phys. Rev. Lett.* **1998**, *81*, 373–376.
- (34) Ryan, A. J.; Fairclough, P. A.; Terrill, N. J.; Olmsted, P. D.; Poon, W. C. K. *Faraday Discuss.* **1999**, *112*, 13–29.
- (35) Wang, Z. G.; Hsiao, B. S.; Sirota, E. B.; Srinivas, S. *Polymer* **2000**, *41*, 8825–8832.
- (36) Meakin, P.; Metiu, H.; Petschek, R. G.; Scalapino, D. J. *J. Chem. Phys.* **1983**, *79*, 1948–1954.
- (37) Keum, J. K.; Zuo, F.; Hsiao, B. S. *Macromolecules* **2008**, *41*, 4766–4776.
- (38) Hu, W.; Frenkel, D.; Mathot, V. B. F. *Macromolecules* **2002**, *35*, 7172–7174.
- (39) Dukovski, I.; Muthukumar, M. *J. Chem. Phys.* **2003**, *118*, 6648–6655.
- (40) (a) Kumaraswamy, G.; Verma, R. K.; Kornfield, J. A. *Rev. Sci. Instrum.* **1999**, *70*, 2097–2104. (b) Kumaraswamy, G.; Kornfield, J. A.; Yeh, F.; Hsiao, B. S. *Macromolecules* **2002**, *35*, 1762–1769. (c) Kornfield, J. A.; Kumaraswamy, G.; Issaian, A. M. *Ind. Eng. Chem. Res.* **2002**, *41*, 6383–6392.
- (41) Seki, M.; Thurman, D. W.; Oberhauser, J. P.; Kornfield, J. A. *Macromolecules* **2002**, *35*, 2583–2594.
- (42) Ogino, Y.; Fukushima, H.; Matsuba, G.; Takahashi, N.; Nishida, K.; Kanaya, T. *Polymer* **2006**, *47*, 5669–5677.
- (43) Matsuba, G.; Sakamoto, S.; Ogino, Y.; Nishida, K.; Kanaya, T. *Macromolecules* **2007**, *40*, 7270–7275.
- (44) Doi, M.; Edwards, S. F. *The Theory of Polymer Dynamics*; Clarendon Press: Oxford, U.K., 1986.
- (45) Van Meerveld, J.; Peters, G. W. M.; Hüller, M. *Rheol. Acta* **2004**, *44*, 119–134.
- (46) Balzano, L.; Rastogi, S.; Peters, G. W. M. *Macromolecules* **2009**, *42*, 2088–2092.

- (47) Balzano, L.; Rastogi, S.; Peters, G. W. M.; Chadwick, J. C. *Phys. Rev. Lett.* **2008**, *100*, 048302–4.
- (48) Keum, J. K.; Zuo, F.; Hsiao, B. S. *J. Appl. Crystallogr.* **2007**, *40*, 48–51.
- (49) Kimata, S.; Sakurai, T.; Nozue, T.; Kasahara, T.; Yamaguchi, N.; Karino, T.; Shibayama, M.; Kornfield, J. A. *Science* **2007**, *316*, 1014–1017.
- (50) D'Haese, M.; Van Puyvelde, P.; Langouche, F. *Macromolecules* **2010**, *43*, 2933–2941.
- (51) Byelov, D.; Panine, P.; Remerie, K.; Biemond, E.; Alfonso, G. C.; De Jeu, W. H. *Polymer* **2008**, *49*, 3076–3083.
- (52) Jerschow, P.; Janeschitz-Kriegl, H. *Int. Polym. Proc.* **1997**, *12*, 72–77.
- (53) (a) Balzano, L.; Rastogi, S.; Peters, G. W. M. *Macromolecules* **2008**, *41*, 399–408. (b) Balzano, L.; Portale, G.; Peters, G. W. M.; Rastogi, S. *Macromolecules* **2008**, *41*, 5350–5355.
- (54) (a) Hagggenmueller, R.; Zhou, W.; Fisher, J. E.; Winey, K. I. *J. Nanosci. Nanotechnol.* **2003**, *3*, 105–110. (b) Hagggenmueller, R.; Fischer, J. E.; Winey, K. I. *Macromolecules* **2006**, *39*, 2964–2971.
- (55) Patil, N.; Balzano, L.; Portale, G.; Rastogi, S. *Macromol. Chem. Phys.* **2009**, *210*, 2174–2187.
- (56) (a) Vega, J. F.; Martinez-Salazar, J.; Trujillo, M.; Arnal, M. L.; Muller, A. J.; Bredeau, S.; Dubois, Ph. *Macromolecules* **2009**, *42*, 4719–4727. (b) Trujillo, M.; Arnal, M. L.; Muller, A. J.; Laredo, E.; Bredeau, St.; Bonduel, D.; Dubois, Ph. *Macromolecules* **2007**, *40*, 6268–6276. (c) Trujillo, M.; Arnal, M. L.; Muller, A. J.; Laredo, E.; Bredeau, St.; Bonduel, D.; Dubois, Ph.; Hamley, I. W.; Castelletto, V. *Macromolecules* **2008**, *41*, 2087–2095.
- (57) (a) Garcia-Gutierrez, M. C.; Hernandez, J. J.; Nogales, A.; Panine, P.; Rueda, D. R.; Ezquerra, T. A. *Macromolecules* **2008**, *41*, 844–851. (b) Hernandez, J. J.; Garcia-Gutierrez, M. C.; Nogales, A.; Rueda, D. R.; Ezquerra, T. A. *Macromolecules* **2009**, *42*, 4374–4376.
- (58) (a) Jain, S. H.; Goossens, J. G. P.; Peters, G. W. M.; van Duin, M.; Lemstra, P. J. *Soft Matter* **2008**, *4*, 1848–1854. (b) Jain, S. H.; Goossens, J. G. P.; van Duin, M.; Lemstra, P. J. *Polymer* **2005**, *46*, 8805–8818.
- (59) (a) Li, L.; Li, C. Y.; Ni, C. *J. Am. Chem. Soc.* **2006**, *128*, 1692–1699. (b) Li, C. Y.; Li, L.; Cai, W.; Kodjie, S. L.; Tenneti, K. K. *Adv. Mater.* **2005**, *17*, 1198–1202.
- (60) (a) Zhang, Q.; Lippits, D. R.; Rastogi, S.; Lemstra, P. J. *Carbon* **2006**, *44*, 778–785. (b) Zhang, Q.; Lippits, D. R.; Rastogi, S. *Macromolecules* **2006**, *39*, 658–666.
- (61) Keum, J. K.; Soman, R. H.; Zuo, F.; Burger, C.; Sics, I.; Hsiao, B. S.; Chen, H.; Kolb, R.; Lue, C. T. *Macromolecules* **2005**, *38*, 5128–5136.
- (62) Wunderlich, B. *Thermal Analysis of Polymeric Materials*; Springer-Verlag: Berlin, 2005.
- (63) Govaert, L. E.; Bastiaansen, C. W. M.; Leblans, P. J. R. *Polymer* **1993**, *34*, 534–540.
- (64) (a) Hermans, P. H.; Platzek, P. *Kolloid-Z.* **1939**, *88*, 68–72. (b) Hermans, P. H.; Weidinger, A. *Makromol. Chem.* **1961**, *44*, 24–36.
- (65) (a) Alexander, L. E. *X-Ray Diffraction Methods in Polymer Science*; John Wiley & Sons: New York, 1969. (b) Roe, R. J. *Methods of X-Ray and Neutron Scattering in Polymer Science*; Oxford University Press: New York, 2000.
- (66) (a) Ruland, W. *J. Polym. Sci., Part C* **1969**, *28*, 143–151. (b) Ruland, W. *J. Appl. Cyst.* **1971**, *4*, 70–73.
- (67) (a) Perret, R.; Ruland, W. *J. Appl. Cyst.* **1969**, *2*, 209–218. (b) Perret, R.; Ruland, W. *J. Appl. Cyst.* **1970**, *3*, 525–532.
- (68) Stribeck, N. *X-Ray Scattering of Soft Matter*; Springer-Verlag: Heidelberg, Germany, 2007.